Polymer 49 (2008) 4635–4646

Contents lists available at ScienceDirect

Polymer

journal homepage: www.elsevier.com/locate/polymer

Synthesis and self-assembling properties of α,ω-hydroxy-poly(ethylene oxide) end-capped with 1-isocyanato-3-pentadecylcyclohexane

Vijay S. Kadam [a], Manohar V. Badiger [a], Prakash P. Wadgaonkar [a], Guylaine Ducouret [b], Dominique Hourdet [b,*]

[a] Polymer Science and Engineering Division, National Chemical Laboratory, Pune 411 008, India
[b] Physico-Chimie des Polymères et des Milieux Dispersés, UMR 7615, ESPCI-CNRS-UPMC, 10 Rue Vauquelin, 75005 Paris Cedex 05, France

ARTICLE INFO

Article history:
Received 18 April 2008
Received in revised form 25 July 2008
Accepted 28 July 2008
Available online 9 August 2008

Keywords:
Associating polymer
Hydrophobically end-capped poly(ethylene oxide)
Star micelles

ABSTRACT

A novel hydrophobic compound, 1-isocyanato-3-pentadecylcyclohexane (PDC) issued from a renewable resource material (Cashew Nut Shell Liquid), is used to end-cap poly(ethylene oxide) (PEO) of different molecular weights. The synthesis, characterization and self-assembling properties of these new associating polymers are reported. In aqueous solution, PDC modified PEOs self-associate into micellar structures which are characterized by neutron scattering. Using a star-polymer model with sticky hard sphere interactions, it is shown that the characteristics of the micelles mainly depend on the size of the PEO chain. In the case of PDC stickers, the aggregation number decreases from 25 to 17 with increasing molecular weight of PEO, from 10 to 20 kg/mol, respectively. The temperature directly impacts the interaction potential between the hydrophilic coronas of PEO which become less repulsive with increasing temperature. Rheological measurements, performed in dilute solution, clearly demonstrate that PEO micelles self-associate into open supramolecular structures. The correlation length of these loose clusters increases with polymer concentration and the hierarchical self-assembly follows the rules of the percolation theory. The sol/gel transition takes place at the overlap concentration of clusters. In semi-dilute solution, the viscoelastic properties of PDC end-capped PEOs are well described by the Maxwell model with a single relaxation mode. The characteristic time of the network follows an Arrhenius temperature dependence with an activation energy of 70 kJ/mol, in very good agreement with the size of PDC stickers.

1. Introduction

Hydrophobically end-capped poly(ethylene oxide)s continue to receive major attention since they form an important class of associating polymers [1–3]. They exhibit unique rheological properties and are used as viscosity modifiers in paints, foods, pharmaceuticals and enhanced oil recovery applications. Moreover, PEO based polymers show low immunogenecity and can be attractive polymers in biomedical applications. Particularly, due to their architectural simplicity with exact location of the associating groups, hydrophobically end-capped PEOs form an ideal model system for fundamental studies of rheology of associating polymers [4–6]. The hydrophilic PEO chain is generally end-capped with hydrophobic stickers (alkyl, perfluoroalkyl or aromatic) attached by ether, ester or urethane linkages [1,7–9]. In dilute aqueous solutions, end-capped PEOs self-assemble and form flowerlike micelles above a critical concentration. The core of the micelle, composed of hydrophobic tails, is surrounded by the loops of hydrophilic PEO. As the polymer concentration increases further, these micelles aggregate and form a transient network characterized by a sharp increase in both viscosity and complex shear modulus. While the elastic modulus depends on the size of the PEO chain and on the polymer concentration, the characteristic time of the network mainly increases with the strength of the association, i.e. the size of the alkyl chain or the ratio of fluorine/hydrogen in perfluoroalkyl [10]. In most cases, the linear viscoelastic behavior of these polymers has been described by a Maxwell model with a single relaxation mode [5,9,11] or two modes [12].

An important category of hydrophobically modified PEO, which has known an industrial development, is Hydrophobically modified Ethoxylated URethane (HEUR) [5]. Initially these polymers were not very well defined from the point of view of their chemical structure (multimodal molecular weight distribution and poor end-capping control) but a lot of efforts have been made to improve their

* Corresponding author. Tel.: +33 (0)1 40 79 46 43; fax: +33 (0)1 40 79 46 40.
E-mail addresses: vijayskadam@gmail.com (V.S. Kadam), mv.badiger@ncl.res.in (M.V. Badiger), pp.wadgaonkar@ncl.res.in (P.P. Wadgaonkar), guylaine.ducouret@espci.fr (G. Ducouret), dominique.hourdet@espci.fr (D. Hourdet).

0032-3861/$ – see front matter © 2008 Elsevier Ltd. All rights reserved.
doi:10.1016/j.polymer.2008.07.064

characteristics. Kaczmarski and Glass have reported on the synthesis of two series of hydrophobically modified HEUR by reacting octadecyl isocyanate and isophorone diisocyanate with PEO [13]. Some of the end-capped PEOs were also prepared by using alkyl tosylate of various hydrocarbon chain lengths [14]. Yao and Jameson synthesized cholesterol end-capped PEOs and studied the influence of rigid hydrophobes on the viscoelastic behavior of these polymers in mixed solvents [15]. Although a well documented literature actually exists on end-capped PEO and their self-assembling properties [8,9,16], there is a vast scope to design and develop novel end-capped PEOs with improved performance, in terms of viscosity and stability towards salts, surfactants and any organic or inorganic compounds involved in most of complex formulations. Moreover, biomass and renewable resources are more than ever a challenging topic for the development of efficient formulations. In this context our main purpose was to develop new associating PEOs on the basis of natural resources like gallic acid, one of the byproducts of tannin industry [17], or cashew nut shell liquid (CNSL).

In a former work [18] we have reported on the synthesis of a new hydrophobic compound, namely 3-pentadecylcyclohexyl amine (3-PDCA), issued from CNSL. In the present paper we describe the synthesis of 1-isocyanato-3-pentadecylcyclohexane (1-IPDC) from 3-PDCA and demonstrate the use of this new hydrophobic compound in the synthesis of novel hydrophobically end-capped PEO.

An important part of this work is dedicated to self-assembling properties of end-capped PEOs in aqueous media. First, the structure and the behavior of PEO aggregates are investigated by neutron scattering. A simple model is applied to describe the micelles of PEO (aggregation number, radius, …) and to analyze the influence of various parameters like polymer concentration, PEO molar mass or temperature on the self-assembled architecture.

The last part of this paper is dedicated to the rheological behavior of PDC end-capped PEO in dilute and semi-dilute solutions. Here we try to correlate the structure and the viscoelastic properties of self-organized PEO micelles. The formation of loose clusters, built up by micellar bridging, is revealed in dilute solution and used to describe the formation of a transient network on the basis of the percolation theory.

2. Experimental section

2.1. Materials

In this study, 3-pentadecyl phenol, Ru/carbon, lithium aluminium hydride (LAH), dibutyltin dilaurate (DBTDL) and pyrene were procured from Aldrich (USA), while Triphosgene was obtained from Anshul chemical Ltd (India). The two poly(ethylene oxide) (PEO) samples with number average molecular weights $M_n \cong 10$ and 20 kg/mol and polydispersity indices of about 1.15 as determined by size exclusion chromatography, were obtained from Fluka. PEO samples were melted and dried under high vacuum for 8 h. Solvents such as isopropanol, chloroform, dichloromethane, ethanol and diethyl ether, toluene (Merck) were purified and dried as per the standard procedures. De-ionized water (Q-Millipore, 18 MΩ) was used for the preparation of polymer solutions and viscometric studies.

2.2. Synthesis of 1-IPDC from 3-PDCA

3-PDCA was synthesized according to the procedure reported in our previous paper [18]. The new hydrophobic compound, 1-IPDC was synthesized from 3-PDCA, as per the following procedure. 3-PDCA (10.0 g, 0.032 moles) was dissolved into 100 ml of dry toluene in a 250 ml three neck round bottom flask equipped with an efficient magnetic stirrer, a thermometer, and an inlet for nitrogen gas and pressure equalizing addition funnel. The flask was flushed with N_2 gas and the amine solution was stirred at 0 °C for 5 min. In another 200 ml flask, 28.84 g of triphosgene (0.097 moles) was weighed and dissolved into 100 mL of dry toluene. The solution of triphosgene was transferred to the addition funnel under N_2 atmosphere and slowly added to the solution of amine with constant stirring for 0.5 h at 0 °C. After the complete addition, the reaction mixture was stirred at room temperature for 2 h and then refluxed for 6 h. Finally an excess of phosgene was removed from the flask, just by flushing the nitrogen and remaining toluene was distilled out under vacuum. Crude product was distilled off under high vacuum to get pure 1-IPDC. The new hydrophobic compound was a low viscous liquid, soluble in toluene, petroleum ether, diethyl ether and chloroform.

2.3. Synthesis of 1-IPDC end-capped PEO

The hydrophobically end-capped PEOs were prepared by the reaction between PEO of different molecular weights and 1-IPDC using dibutyl tin dilaurate as a catalyst. Since the reaction is moisture sensitive, all the glasswares were oven dried before use. In a typical procedure, a 500 mL three-necked flask equipped with Dean–Stark apparatus, magnetic stirring bar, thermometer and an inlet for nitrogen gas, was flushed with nitrogen gas. Pre-dried PEO (10.0 g, 1 mmol) ($M_n = 10$ kg mol^{-1}) and 250 mL of dry toluene was charged into the reaction flask. The solution was heated in an oil bath at 50 °C. Any trace of moisture present in PEO was removed by distilling off toluene azeotropically to an extent that there remains approximately 100 ml of toluene in the reaction flask. When PEO was completely dissolved in toluene, 2.01 g (6 mmol) of 1-PDIC dissolved separately in 50 mL of dry toluene was added to the flask slowly by using cannula. Dibutyl tin dilaurate (DBTDL, 0.5 mL) was added as a catalyst and the reaction was carried out for 12 h at 100 °C under nitrogen atmosphere. After 12 h, a second lot of 1-IPDC (4 mmol) was added to the flask and the reaction was further carried out for another 24 h at 100 °C. An excess amount of 1-IPDC ensured complete end capping of PEO. The reaction mixture (250 mL) was precipitated out in 3 l of petroleum ether. The white powder like precipitate was then filtered and dried under reduced pressure. In order to purify further, the white powder was redissolved in warm acetone and then filtered through 1 μm syringe filter and slowly precipitated into petroleum ether. This redissolution and reprecipitation step was repeated several times to obtain the pure polymer. Two end-capped PEO were prepared following the above procedure and these were designated as PEO10K-PDC and PEO20K-PDC, where 10K (or 20K) is the molar mass of PEO 10 kg/mol (or 20 kg/mol) and PDC are the α,ω-pentadecylcyclohexyl end groups.

2.4. Sample preparation

The polymer solutions in gram per liter (g L^{-1}) of the desired concentration (C) were prepared by directly dissolving a known amount of polymer into de-ionized water. Each solution was gently stirred at room temperature to get a clear homogenous solution. The gel samples were allowed to homogenize for 2–3 days and gently rotated further for 2 more days. All the solutions and gel samples were optically clear after complete dissolution.

2.5. Characterization

2.5.1. NMR spectroscopy

The ^{1}H NMR spectra of 1-IPDC and end-capped PEO were recorded on a Bruker DRX-500 NMR spectrometer operating at proton frequency of 500 MHz. The NMR spectra of 1-IPDC and polymer samples were taken in $CDCl_3$.

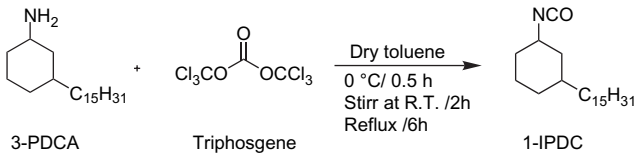

Scheme 1. Synthesis of hydrophobic compound (1-IPDC) from 3-PDCA.

2.5.2. Capillary viscometry

Intrinsic viscosities of PEO precursors and PDC end-capped PEO were determined by capillary viscometry using an automatic Ubbelohde viscometer (SEMATech Til). For all the polymers, initial stock solutions were prepared at a concentration $C = 20\ \mathrm{g\,L^{-1}}$ and the experiments were carried out in water at a controlled temperature: $T = 20\ ^{\circ}\mathrm{C}$.

2.5.3. Rheology

Flow properties of dilute samples were measured on a Contraves Low-Shear 30 rheometer equipped with stainless steel coaxial cylinders (radius of the cup: 6 mm, radius of the conical bob: 5.5 mm).

Dynamic and steady state measurements were performed on a strain-controlled rheometer (TA Instruments ARES LS1) equipped with cone and plate geometry (diameter: 50 mm, angle: 0.04 rad, gap: 50 μm) made by titanium and stainless steel, respectively. First, the sample was submitted to a short strain sweep at a fixed frequency (1 Hz) to determine the range of linear response. The strain sweep, stopped before reaching the beginning of the nonlinear regime, was followed by a frequency sweep. The storage (G') and loss (G'') moduli were measured in the linear viscoelastic regime for frequencies ranging from 0.01 to 100 rad/s. Then, a total strain sweep was performed at 1 Hz up to the maximum strain amplitude. All the measurements were carried out at temperatures ranging from 5 to −30 °C.

2.5.4. Small angle neutron scattering (SANS)

SANS experiments were performed at Laboratoire Léon Brillouin, Saclay (France). An incident neutron beam of wavelength $\lambda = 12$ Å was selected with a corresponding sample-to-detector distance of 1.67 m. This configuration provides a scattering vector modulus $[q = (4\pi/\lambda)\sin(\theta/2)]$ ranging between 0.01 and 0.1 $\mathrm{Å^{-1}}$ (θ is the scattering angle). Polymer solutions were prepared at room temperature in D_2O and transferred between 2 quartz plates separated by a 2-mm-thick spacer. To obtain the coherent scattering intensity of the polymer, the signal given by the solvent, used as background, was subtracted from the scattering intensity of the polymer sample. The efficiency of the detector cell was normalized by the intensity delivered by a pure water cell of 1-mm thickness. Absolute measurements of the scattering intensity $I(q)$ ($\mathrm{cm^{-1}}$ or $10^{-8}\ \mathrm{Å^{-1}}$) were obtained from the direct determination of the incident neutron flux and the cell solid angle. The length scattering densities of D_2O, PEO and PDC end groups are $\rho = 6.38$, 0.66 and −0.38 ($10^{-6}\ \mathrm{Å^{-2}}$), respectively.

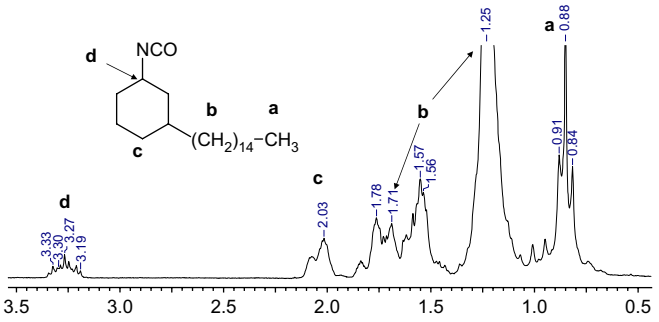

Fig. 2. ^{1}H NMR spectrum of 1-IPDC.

3. Results and discussion

3.1. Synthesis and characterization

3.1.1. 1-IPDC

The detailed procedure of the synthesis of 3-PDCA has been reported previously [18]. In order to get a better reactivity between hydrophobe molecules and PEO end groups, we have converted in the present work the 3-PDCA precursor into 1-IPDC using a single step reaction with triphosgene (see Scheme 1).

The chemical structure of 1-IPDC was qualitatively confirmed by FT-IR. As shown in Fig. 1, the strong stretching vibration band at 2261 $\mathrm{cm^{-1}}$, clearly indicates the presence of isocyanate group (–NCO).

The chemical structure of 1-IPDC has been resolved by ^{1}H NMR (see Fig. 2). The triplet of the terminal methyl proton ($-CH_3$) of the pentadecyl chain clearly appears at 0.88 ppm (t, 3H, $-CH_3$). The aliphatic protons of the pentadecyl chain (CH_2) and the cyclohexyl ring ($-CH_2$ and –CH) fall in the range of 1.0–2.1 ppm. Finally, the methine proton of the cyclohexyl ring attached to the carbon covalently bonded to the isocyanate group appears at 3.27 ppm.

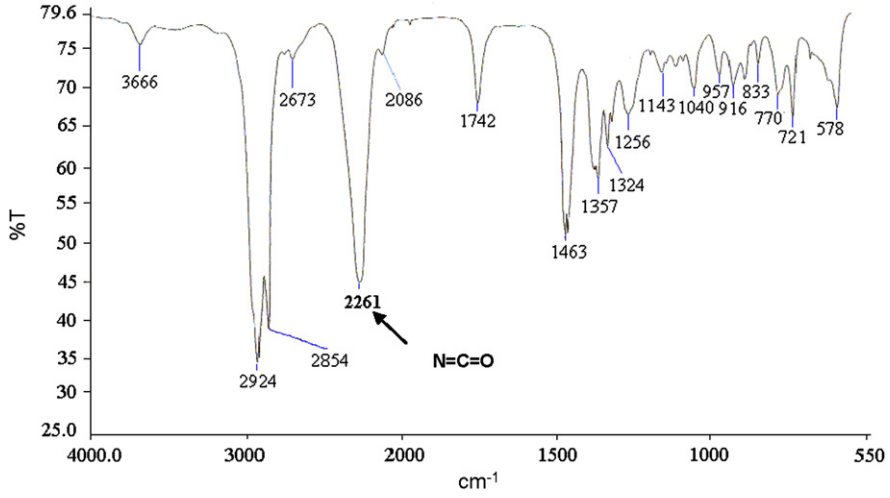

Fig. 1. FT-IR spectrum of 1-IPDC.

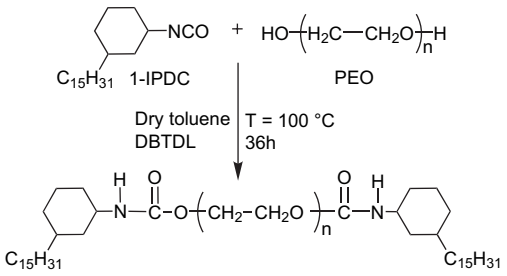

Scheme 2. Synthesis of 1-IPDC end-capped PEO.

3.1.2. End-capped PEO

We have synthesized hydrophobically end-capped PEO by reacting PEO of two different molecular weights (10K and 20K) with 1-IPDC. The reaction pathway is shown in Scheme 2. Since the reaction between the –OH groups of PEO and –NCO groups of 1-IPDC is fast and further catalyzed by DBTDL, a total completion of the reaction is ensured with no detectable side reactions leading to the formation of byproducts. Furthermore, by varying the molecular weight of PEO one can change the hydrophilic/hydrophobic balance of the polymer to get the desired properties.

The end-capping efficiency was calculated by ^{1}H NMR spectroscopy using the intensity ratio between hydrophobe and ethylene oxide protons, respectively (see Table 1).

The results clearly indicate that PEO10K is quantitatively modified by introducing hydrophobic PDC groups at both ends of the chain. We can also consider that the same holds for the PEO20K even if the characterization gives an end-capping efficiency of about 95%. This small discrepancy is mainly due to the very small molar ratio of protons between hydrophobic stickers and PEO chain of high molecular weight.

3.2. Associating behavior of end-capped PEO in aqueous solutions

3.2.1. Small angle neutron scattering (SANS)

SANS experiments were carried out at different temperatures ($T = 20$–40 °C) with solutions of PEO10K-PDC and PEO20K-PDC in heavy water, D_2O ($C = 20$–60 g/L). As we will see later, the percolation threshold of PDC end-capped PEO takes place in this concentration range and we can reasonably assume that polymeric micelles do not strongly overlap in these conditions. If we suppose that hydrophobically end-capped PEOs self-associate into flower-like micelles of volume V, which interact between them with a potential of spherical symmetry, the scattered intensity $I(q)$ can be written as follows:

$$I(q) = nV^2(\Delta\rho)^2 P(q)S(q) \quad (1)$$

with q the scattering vector, n the number density of scatterers (micelles), $\Delta\rho$ the contrast factor, $P(q)$ the form factor of the micelle and $S(q)$ the structure factor that takes into account the interactions between the aggregates.

Table 1
End-capping efficiency of hydrophobically end-capped PEOs determined from ^{1}H NMR spectroscopy

PEO	End group	Designation	K_{theo}	K_{exp}	PDC/chain	Y (%)
10K	PDC	PEO10K-PDC	0.081	0.081	2.0	100
20K	PDC	PEO20K-PDC	0.040	0.037	1.9	93

Y: end-capping efficiency; K_{theo}, K_{exp}: theoretical and experimental proton ratios between hydrophobic stickers and hydrophilic PEO (protons a and d of PDC are not taken into account: see Fig. 2).

Starting from this relation, scattering intensities can be interestingly plotted versus q after normalization with respect to the concentration ($I(q)/C \sim I(q)/n$) as shown in Fig. 3. For each end-capped polymer we get a "master" curve, which depicts the scattering of aggregates of similar morphology in the range of concentration explored. In order to describe the scattering behavior of solution of PEO micelles, we will use the picture given in Fig. 3 of a starlike micelle with N_{sti} arms organized into concentric shells of close-packed blobs. In the high q range, where the internal structure of the blobs is probed, the scattering intensity follows a $q^{-\alpha}$ law for the two polymers. The exponent α takes into account the balance between attractions and repulsions taking place between monomer units of the polymer [19]: $\alpha > 2$ if the attractions between monomer units prevail (as for collapsed polymer chains or globular conformation), $\alpha < 2$ if repulsions between monomer units dominate (polymer in good solvent) and $\alpha = 2$ if the forces vanish (case of the Gaussian coil). For PEO20K-PDC, we obtain a low value of the scaling coefficient ($\alpha = 1.7 \cong 5/3$) which means that excluded volume interactions still exist between EO units inside the blob as it is the case for pure PEO in water [20]. Conversely the scattering behavior of PEO10K-PDC shows stronger attractions between EO units: $\alpha = 2.5$. This high coefficient can be explained by taking into account, for a given type of sticker, the increasing hydrophobicity of PEO–PDC with decreasing molecular weight of the PEO chain. Following this argument, which has been investigated in more detail by Grassl et al. [16], a phase separation is expected for PEO–PDC of lower molecular weights.

In the intermediate q range: $R_{Star}^{-1} < q < \xi_{max}$ where, R_{Star} is the radius of the star and ξ_{max} is the size of the larger blob, a higher q-dependence is observed for the two polymers ($\alpha = 3.5$) in agreement with the theoretical values ($\alpha = 3$–4) calculated from the Gaussian star model of Benoît [21] or the spherical brush model of Daoud and Cotton [22]. These high values of the scaling behavior mirror the higher compactness or internal density of stars compared to linear polymers.

Finally, in the low q range, an increasing drop of the intensity is observed with increasing concentration along with the progressive appearance of a correlation peak. The relative position of the maxima (q_{max}) is shifted towards higher q values when the concentration increases. By considering this maximum as a Bragg

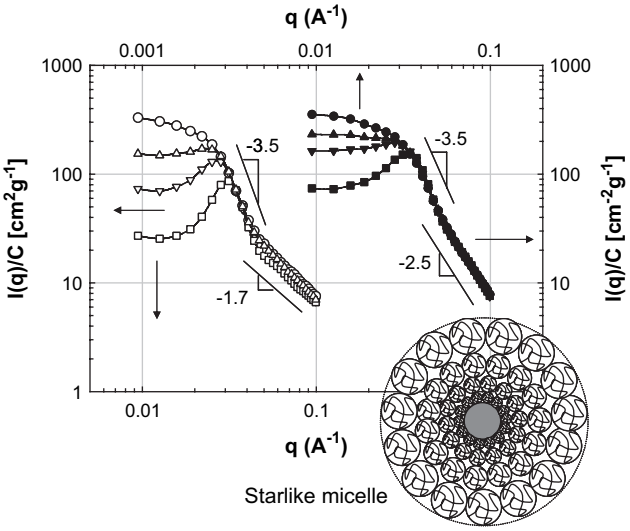

Fig. 3. Scattered intensity (reduced by the concentration) for PEO10K-PDC (filled symbols) and PEO20K-PDC (open symbols) solutions in heavy water ($T = 20$ °C). $C = 20$ g L^{-1} (○ ●), $C = 30$ g L^{-1} (△ ▲), $C = 40$ g L^{-1} (▽ ▼) and $C = 60$ g L^{-1} (□ ■). Lines are guides for the eye.

peak, q_{max} can be used to estimate the average distance between the centers of neighboring scatterers:

$$D = 2\pi/q_{max} \quad (2)$$

Moreover, if we consider a liquid order with micelles organized into a simple cubic lattice, one can obtain the average concentration of micelles and the number of stickers per micelle (N_{sti}) assuming that all the stickers are embedded inside hydrophobic clusters. As there are two stickers per PEO chain, we can define the average number of polymer chains associated to one micelle (N_{agg}) as:

$$N_{agg} = N_{sti}/2 \quad (3)$$

The characteristic parameters calculated from this assumption are reported in Table 2 for the two polymers at different concentrations. This qualitative treatment of the scattering data gives interesting information concerning the morphology of the aggregates. For instance, we can verify that the aggregation number strongly depends on the hydrophilic/hydrophobic balance [16].

In the present study, N_{agg} decreases as expected with increasing size of the PEO chain (23–27 for PEO10K-PDC to 15–18 for PEO20K-PDC). For an isotropic solution of micelles with constant aggregation number, q_{max} is expected to vary with the concentration as C^a, with $a = 1/3$. In the present case the exponent is quite close, although a little bit larger ($a = 0.45$). The uncertainty on this exponent can be attributed to the small collection of data and to the low accuracy on the exact position of q_{max}.

Many attempts have been made to model SANS data of block copolymers like PEO–PPO–PEO [23–25] and hydrophobically end-capped PEOs. In this context we can underline the study of Porte and coworkers [26,27] as well as those of François and coworkers [28,29], which have given a very detailed description of the structure of α- and α,ω-end-capped PEOs in dilute and semi-dilute solutions. All these studies proceed similarly and try to draw a physical and realistic description of macromolecular assemblies using adequate functions for $P(q)$ and $S(q)$.

In our systems, two different scattering species are present: aliphatic PDC end groups, embedded into the core of the aggregate (index c), and PEO chains which form the corona of the micelle (index s). In D_2O, where no part of the polymer is matched, the scattered intensity contains three different terms:

$$I(q) = nV_c^2(\Delta\rho_c)^2P_c(q)S_c(q) + nV_s^2(\Delta\rho_s)^2P_s(q)S_s(q) + X \quad (4)$$

with V_c and V_s the volumes of hydrophobic core and PEO shell, respectively, and $\Delta\rho_c$ and $\Delta\rho_s$ their contrast factors, i.e. the difference of length scattering densities between core, or shell, and their surrounding media.

$X \sim V_cV_s\Delta\rho_c\Delta\rho_s$ is the term accounting for the cross-correlations between scattering species (core and corona). Due to the very low weight fraction of hydrophobic end groups, $V_s^2(\Delta\rho_s)^2$ is more than 100 times higher than $V_c^2(\Delta\rho_c)^2$ in D_2O solutions and more than 20 times higher than $V_cV_s\Delta\rho_c\Delta\rho_s$. Consequently, we will only consider the second term of Eq. (4) in the following and we will use the form factor of a Gaussian star [21] to describe the conformational structure of PEO chains inside the corona:

Table 2
Self-assembling characteristics of end-capped PEO micelles in aqueous solutions

Sample	PEO10K-PDC		PEO20K-PDC		
C (g L^{-1})	40	60	30	40	60
q_{max} (Å)$^{-1}$	0.028	0.034	0.023	0.027	0.031
D (Å)	224	185	273	235	203
N_{agg}	27	23	18	16	15

The values are calculated from the scattering maxima (q_{max}).

$$P_s(q) = \frac{2}{x^2}\left[\frac{f}{2}(f-1)\exp(-2x/f) - f(f-2)\exp(-x/f) + x + \frac{f}{2}(f-3)\right] \quad (5)$$

with

$$x = (qR_{g,\,Star})^2\frac{f^2}{3f-2} \quad (6)$$

where, f is the number of arms ($f = N_{sti} = 2N_{agg}$ in the present case) and $R_{g,\,Star}$ is the radius of gyration of the whole star which is related to that of one arm ($R_{g,\,arm}$) by:

$$R_{g,\,Star}^2 = \frac{(3f-2)}{f}R_{g,\,arm}^2 \quad (7)$$

Within the Gaussian approximation, the radius of the Gaussian star R_{Star} can be estimated by:

$$R_{Star} = R_{g,\,Star} \quad (8)$$

As seen in Fig. 3, interactions between flowerlike micelles give rise to a correlation peak which increases with polymer concentration. In order to take into account steric repulsions between PEO coronae and bridging attractions, we use the Baxter's model which explicitly describes the short range interactions between hard spheres with adhesive surfaces [30]. The pairwise interparticle interaction potential of such particles is shown in Fig. 4, with R_{HS} the inner radius of the hard sphere and R the radius of the adhesive sphere. The expression $2R$–$2R_{HS}$ corresponds to the thickness of the adhesive surface layer, or the width of the attractive well.

$$\frac{u(r)}{kT} = \begin{cases} \infty & \text{for} \quad 0 < r < 2R_{HS} \\ \lim\limits_{R\to R_{HS}} \ln\left[12\zeta\left(\frac{R-R_{HS}}{R}\right)\right] & \text{for} \quad 2R_{HS} < r < 2R \\ 0 & \text{for} \quad 2R < r \end{cases} \quad (9)$$

On the basis of this interaction potential consisting of a hard core together with a rectangular attractive well, Baxter solved the Percus-Yevick approximation, provided that a certain limit is taken (see Eq. (9)) in which the range of the well becomes zero ($R = R_{HS}$) and its depth infinite in such a way that the "stickiness parameter" (ζ^{-1} in k_BT units) remains finite. The interparticle structure factor ($S_s(x)$) is then given analytically by:

$$\frac{1}{S_s(x)} - 1 = 24\phi_{HS}\left(\alpha f_2(x) + \beta f_3(x) + \frac{\alpha}{2}\phi_{HS}f_5(x)\right) + 2\phi_{HS}^2\lambda^2 f_1(x) - 2\phi_{HS}\lambda f_0(x) \quad (10)$$

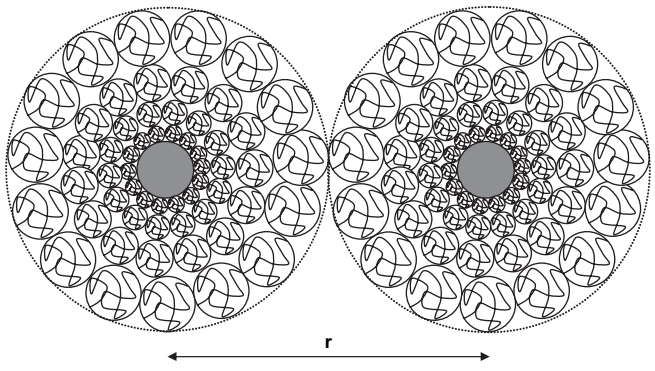

Fig. 4. Interparticle interaction potential between hard spheres with adhesive surfaces.

where ϕ_{HS} is the volume fraction of hard spheres, α, β and λ, are parameters which depend on ϕ_{HS} and ζ^{-1}, and f_0, f_1, f_2, f_3, and f_5, are trigonometric functions of $x = 2qR$ [see Refs. [24,30]].

According to this model of Gaussian stars behaving as sticky hard spheres, we have to consider four adjustable parameters (R_{Star}, N_{sti}, R_{HS}, and ζ^{-1}) while all the others (polymer concentration, molar mass, contrast factor, etc.) are fixed by the experiment. For instance, the volume fraction of hard spheres (ϕ_{HS}) and the number density of micelles (n) can be obtained from the following relations:

$$\phi_{HS} = \frac{4\pi N_{Avo} C w_{sti} R_{HS}^3}{3 M_{sti} N_{sti}} \tag{11}$$

and

$$n = \frac{3\phi_{HS}}{4\pi R_{HS}^3} \tag{12}$$

where, N_{Avo} is the Avogadro number, C the polymer concentration (in weight per volume), w_{sti} the weight fraction of hydrophobic stickers in the end-capped polymer and M_{sti} the molar mass of the hydrophobic sticker.

On the basis of Eq. (4), a nonlinear curve fitting was applied to fit the SANS intensities in absolute scale. Whatever is the polymer solution, the procedure converges on a single set of variables: R_{Star}, N_{sti}, R_{HS}, and ζ^{-1}. An illustration is given in Fig. 5 with solutions of PEO10K-PDC and the fitting parameters are reported in Table 3.

First of all, we can observe a very good agreement between experimental data and model fittings for all concentrations. Contrary to solutions of α-modified PEOs [25] or pluronics [28] for which the scattering behavior can be modeled by considering hard sphere repulsions between micelles, the situation is different with α,ω-end-capped PEOs which form intermicellar bridges. From Fig. 6, where the best fittings obtained with a simple hard sphere potential (dash line) or an adhesive hard sphere potential (solid line) are compared, we can see clearly that the physical description of attractions through the Baxter's model is necessary to really fit the data on the whole range of q. This is especially true at high concentrations ($C = 40\ g\ L^{-1}$ and $60\ g\ L^{-1}$) where interactions prevail. Even if the fit is not perfect, especially in the high q range where other contributions of Eq. (4) are lacking, this model really captures the main features of end-capped PEO self-assembling.

From Table 3, we can see that PEO10K-PDC form star micelles characterized by a radius $R_{Star} \cong 71$ Å. The radius of the micelles

Table 3
Self-assembling characteristics of end-capped PEO micelles in aqueous solutions

Sample		PEO10K-PDC				PEO20K-PDC			
C (g L^{-1})		20	30	40	60	20	30	40	60
R_{Star} (Å)		71	71	71	71	99	100	103	100
R_{HS} (Å)	$T = 20$ °C	84	95	100	101	100	129	127	122
	$T = 40$ °C	–	83	94	95	100	124	123	120
N_{agg}		18	20	22	26	14	16	17	19
ζ^{-1} (k_BT)		8	12	13	17	9	13	13	21

The fitting parameters are calculated from the Gaussian star model with sticky hard sphere repulsions.

remains constant with increasing concentration while the number of stickers per micelle smoothly increases, from $N_{agg} = 19$–26 between $C = 20\ L^{-1}$ and $60\ g\ L^{-1}$. According to this model, the star micelles interact with each other with a hard sphere radius $R_{HS} = 84$–100 Å and a stickiness parameter $\zeta^{-1} = 8$–$16\ k_BT$. The latter is similar to the values reported by Pham and coworkers [31,32] in the case of PEO end-capped with C16 or C18 ($\zeta^{-1} = 11$ and $15\ k_BT$, respectively). Above $20\ g\ L^{-1}$, the structural parameters are very close and do not show a strong concentration dependence. In the case of PEO20K-PDC, the conclusions are qualitatively the same except that the size of the stars is greater $R \cong 100$ Å and the aggregation number is lower $N_{sti} = 14$–19.

We can notice that these aggregation numbers are in good agreement with the approximation made from q_{max} (see Table 2). They are significantly smaller than those commonly found for nonionic micelles with shorter ethylene oxide chains but in good agreement with those reported for hydrophobically end-capped PEOs. Of course, the differences arise from internal structure of the polymer (PEO chain length, nature and size of the hydrophobic group, nature of the spacer) but also from the polymer concentration or the experimental technique used for the determination (Dynamic Light Scattering, Time-Resolved Fluorescence Quenching) [33]. In the case of PEO ($M_w \cong 35\ kg\ mol^{-1}$) end-capped with $C_{16}H_{33}$ hydrophobe, the following functionalities have been reported: $N_{sti} = 18$ by Yekta et al. [9] $N_{sti} = 21$ ($C < 10\%$) and 35 ($C > 10\%$) by Vorobyova et al. [34], $N_{sti} = 40$ by Pham et al. [31] and $N_{sti} = 34$ by Beaudoin et al. [28].

The influence of the temperature on the behavior of PEO stars is given in Fig. 7, where the scattering intensity of PDC end-capped PEO solutions ($C = 40\ g\ L^{-1}$) has been plotted versus q for different temperatures.

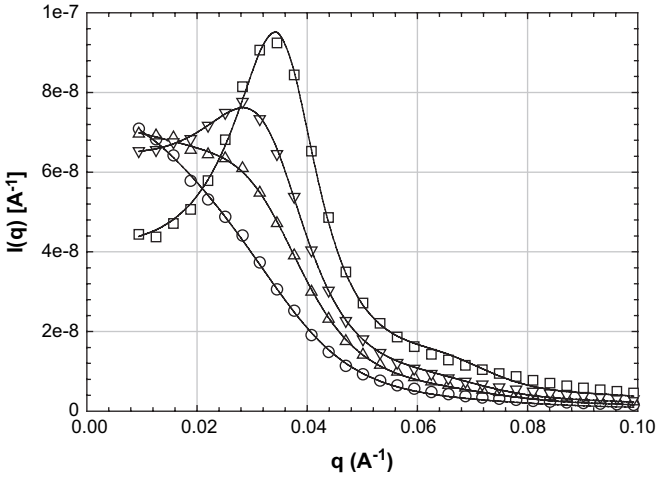

Fig. 5. Experimental (symbols) and calculated (solid lines) scattering intensities for solutions of PEO10K-PDC at different concentrations (D_2O – $T = 20$ °C). $C = 20\ g\ L^{-1}$ (○), $C = 30\ g\ L^{-1}$ (△), $C = 40\ g\ L^{-1}$ (▽) and $C = 60\ g\ L^{-1}$ (□).

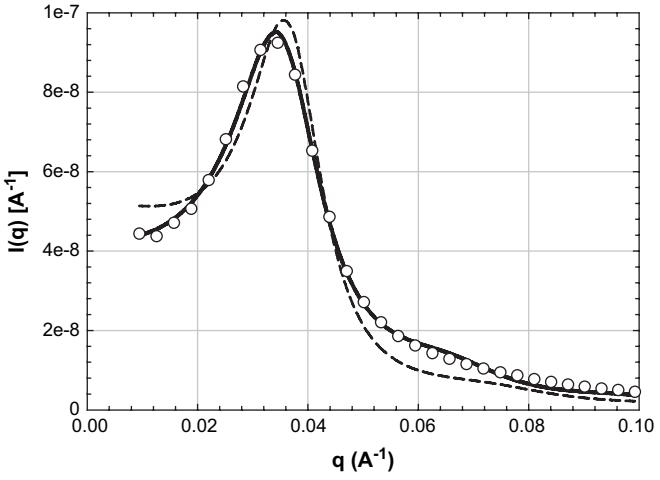

Fig. 6. Experimental (○) and calculated (lines) scattering intensities for a solution of PEO10K-PDC ($C = 40\ g\ L^{-1}$ – D_2O – $T = 20$ °C). The dash line has been calculated using a hard sphere potential while the solid one is obtained assuming adhesive hard sphere interactions.

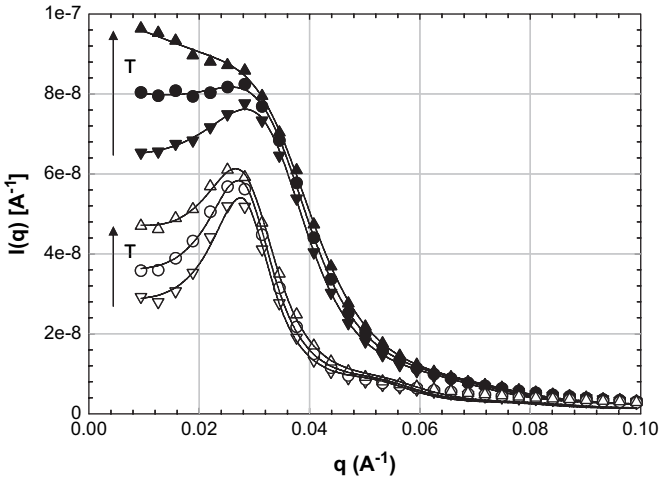

Fig. 7. Experimental scattering intensities for solutions of PEO10K-PDC (filled symbols) and PEO20K-PDC (open symbols) aqueous solutions ($C = 40\ g\ L^{-1}$) at different temperatures: $T = 20\ °C$ (▽ ▼), $T = 30\ °C$ (○ ●), $T = 40\ °C$ (△ ▲). The fits obtained from the previous model (solid lines) are plotted in absolute intensity scale.

This scattering pattern with temperature is representative of all scattering curves obtained with the two end-capped PEO at all concentrations. Qualitatively, the increase of temperature weakens the repulsions between the starlike micelles. This is attributed to the deswelling of the PEO corona as the solvent quality of water decreases with temperature ($\Theta = 100\ °C$). Quantitative results obtained by fitting the experimental data (see Fig. 7 and Table 3), indicate that all the parameters remain almost unchanged in this small range of temperatures, except R_{HS} which clearly decreases upon heating ($\Delta R/R = 3$–5% between 20 and 40 °C). This behavior has been reported with other associating systems containing hydrophilic PEO block, like HEUR [28], pluronics [25] or nonionic surfactant like Brij-35 ($C_{12}EO_{23}$) [35].

3.3. Rheology

3.3.1. Introduction

The concentration dependence of relative viscosities of hydrophobically end-capped and unmodified PEOs is presented in Fig. 8. At low concentrations ($C < 20\ g\ L^{-1}$) the measurements were carried out with both capillary and low-shear viscometers while at higher concentrations ($C > 20\ g\ L^{-1}$) Newtonian viscosities were obtained using a control strain rheometer. As we can see, the association of PDC modified PEO in aqueous solution gives rise to a sharp increase in viscosity above a concentration threshold that depends on the molar mass of PEO.

This behavior is similar to that predicted by Semenov et al. [36] for α,ω-end-capped associating polymers and to those observed with similar modified PEOs [11,16,26]. Prior to study the gelation process of these systems and their viscoelastic properties in the "gel regime", we will first investigate the behavior of these polymers in dilute solutions, typically below 10–20 $g\ L^{-1}$.

3.3.2. Dilute solution properties

An important parameter, which characterizes the specific volume of swollen polymer chains in dilute solution, is the intrinsic viscosity ($[\eta]$). This parameter is generally obtained by plotting the viscometric data according to the well-known Huggins relation:

$$\eta_{sp}/C = \frac{\eta - \eta_s}{\eta_s C} = \frac{t - t_s}{t_s C} = [\eta] + k_H[\eta]^2 C \qquad (13)$$

where, η is the viscosity of the solution, η_s is the viscosity of the solvent, t and t_s are the flow times measured with the capillary viscometer for the polymer solution and solvent, respectively, C is the polymer concentration, k_H is the Huggins coefficient and η_{sp}/C is the reduced viscosity.

This relation works perfectly well in the case of PEO precursors but it fails with PDC modified PEOs as we get a deviation from the linearity at very low concentration. This is shown in Fig. 9 where we have plotted the ratio of the reduced viscosity, between the modified sample and its precursor versus the polymer concentration.

By comparing the two associating polymers, PEO20K-PDC clearly displays the stronger viscosity enhancement, as the viscosity starts to diverge for $C > 10\ g\ L^{-1}$. In the same concentration range, the reduced viscosity of PEO10K-PDC is always higher than that of PEO10K but their ratio still remain below 4 even at $C = 20\ g\ L^{-1}$. In these conditions, it is not possible to apply the Huggins relation to extrapolate the intrinsic characteristics of the systems and we follow the treatment proposed by Fedors [37]. This has been successfully applied to macromolecular systems, which display a strong concentration dependence of their hydrodynamic properties, like for instance associating polymers [38,39]. Initially developed to describe the viscosity of Newtonian suspensions of rigid particles, Fedors has shown on the basis of a large set of experimental data that the following equation can be applied to relative viscosities ($\eta_r = \eta/\eta_s$) ranging between 1 and 100:

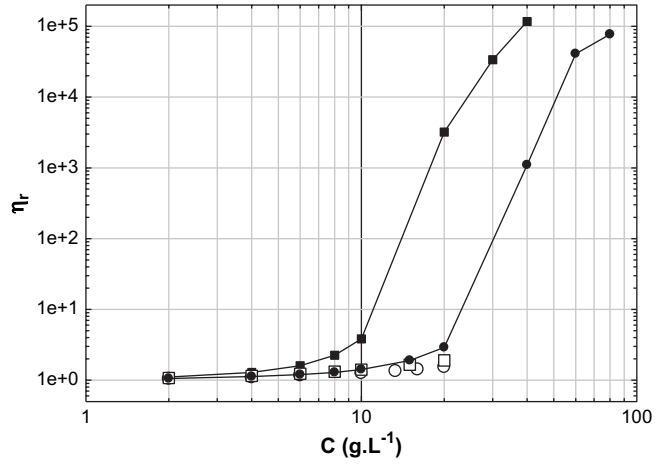

Fig. 8. Relative viscosity ($\eta_r = \eta_{solution}/\eta_{solvent}$) of PEO derivatives in aqueous solution ($T = 20\ °C$): PEO10K (○), PEO10K-PDC (●), PEO20K (□), PEO20K-PDC (■).

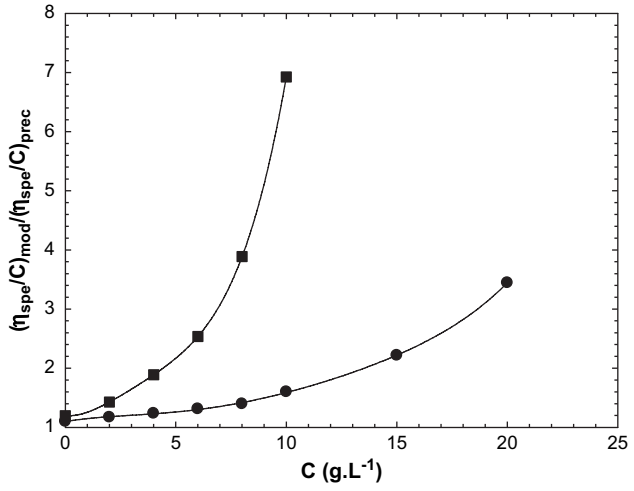

Fig. 9. Reduced viscosity ratio between end-capped PEOs and their precursors versus polymer concentration ($T = 20\ °C$): PEO10K-PDC (●), PEO20K-PDC (■).

$$\frac{1}{2\left(\eta_r^{1/2}-1\right)} = \frac{1}{[\eta]}\left(\frac{1}{C}-\frac{1}{C_m}\right) \quad (14)$$

In this relation, the concentration parameter C_m has the same meaning as ϕ_m for solid particles, which is the maximum packing fraction.

As shown in Fig. 10, the Fedors treatment gives a very good linearization of the data for all the polymers ($r > 0.999$), and the main parameters obtained from this representation are given in Table 4.

First of all we can see that the intrinsic viscosities of PDC end-capped PEO are slightly higher compared to those of their respective precursors. This means that the supra-macromolecular structures formed in this concentration range have similar or higher specific volumes compared to the swollen PEO precursors. Obviously, these structures cannot be isolated flowers as these objects have a higher density than their precursors. As a matter of fact, the flowerlike micelle model [36] predicts the volume per chain to decrease as $R_{Star}^3/N_{agg} \sim N_{agg}^{(1-3\nu)/2}$, with the Flory exponent $\nu = 0.5$–0.6 in Θ-conditions or in good solvent, respectively. Under these considerations the expected specific volume (or intrinsic viscosity) of flowerlike micelles should be two or three times lower than that of the corresponding PEO.

A similar behavior has been reported in dilute solutions for other PEOs end-capped with perfluoroalkyl [40] or alkyl groups [41] and these results point out that macromolecular structures formed in dilute solutions are more probably fractal aggregates (clusters) built from flowerlike micelles as pictured in Fig. 11.

This schematic representation is in good agreement with the scattering picture given by SANS with starlike micelles interacting with an adhesive hard sphere potential. It also takes into account the literature background on telechelic polymers. Hydrophobically end-capped PEOs are effectively known to strongly self-associate at low concentrations, giving rise to the formation of flower-like micelles above the c.a.c. These flowers are expected to form cooperatively following a closed association model [41]. After this initial step, the formation of intermicellar bridges causes an effective attractive potential, which leads to a progressive and reversible aggregation of micelles into loose clusters. This second step corresponds to an open association process [41], which is similar to the aggregation behavior taking place between adhesive spheres [42]. When the concentration of polymer increases, the fractal clusters percolate and form a transient network of flowers, which induces a strong increase of viscosity.

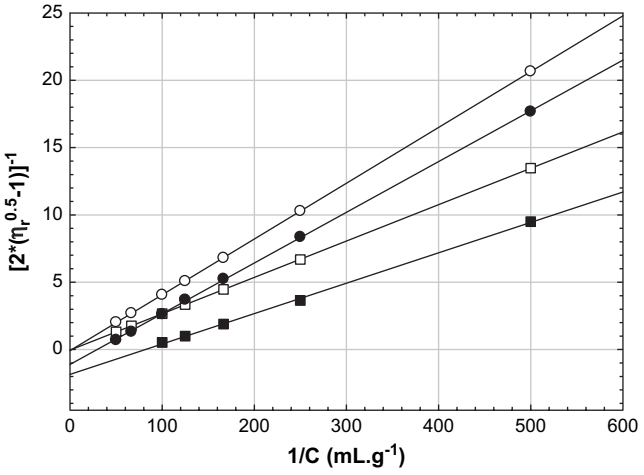

Fig. 10. Fedors plot applied to hydrophobically end-capped PEO (filled symbols) and their precursors (hollow symbols): $T = 20$ °C, PEO10K series (○ ●), PEO20K series (□ ■).

Table 4
Intrinsic viscosity ($[\eta]$) and packing concentration (C_m) extrapolated for PEO samples in dilute solution

Sample	$[\eta]$ (mL g^{-1})	C_m (g mL^{-1})	C^* (g mL^{-1})
PEO10K	24.2	0.55	0.032
PEO10K-PDC	26.6	0.034	0.029
PEO20K	37.0	0.68	0.021
PEO20K-PDC	44.3	0.013	0.017

The overlap concentration C^* is calculated on the basis of a simple cubic lattice of spheres: $C^* = 0.76/[\eta]$.

As mentioned by Bremer et al. [43] in the case of casein aggregation, the point of gel formation (C_g) can be determined from the intrinsic viscosity of fractal clusters, by calculating their overlap concentration ($C^* \sim 1/[\eta]$, see Table 4). The values calculated according to this criterion are in good agreement with the strong deviation of viscosity observed in Fig. 9 for the two end-capped polymers. Nevertheless, the problem with fractal clusters is that their density (d) decreases as their size ($R_{cluster}$) increases: $d \sim R_{cluster}^{D-3}$, with D the fractal dimension which is less than the geometric dimension of 3. Accordingly, the intrinsic viscosities extrapolated for associating PEO only capture the density of intermediate clusters.

Another estimation of C_g can be done by using the equation of Fedors and assuming that $C_m \cong C_g$. This assumption seems quite reasonable as C_m normally corresponds to the maximum packing concentration in the case of hard spheres. Above this concentration a huge increase of viscosity is expected for hard spheres and for associating polymers as well. Unlike C^*, which was extrapolated from average structures formed in the course of the aggregation process, C_m should be closer to the overlap criterion assumed for the percolation threshold. The C_m values, given in Table 4, are in good agreement with the viscosity behavior of end-capped PEO. They are also very close to C^* and taking into account the uncertainty in the extrapolation of these concentrations, we will consider that $C_m \cong C^* \cong C_g$ and in the following we will average these parameters to define the gel point: $C_g = (C_m + C^*)/2$.

By comparison, the C_m values calculated from hydrophilic PEO solutions are very high. As these polymers do not exhibit strong increase of viscosity in the range of concentrations explored, the C_m values are shifted towards very high concentrations without strong meaning for the extrapolated values. The point is that when $C \ll C_m$, the Fedors equation simply reduces to Huggins relation with $k_H = 0.25$.

3.3.3. *Viscoelasticity of polymer solutions at and above* C_g

3.3.3.1. Dynamic moduli. The viscoelastic properties of hydrophobically end-capped PEO solutions have been described in terms of transient network theory. This theory was first introduced by Green and Tobolsky [44] and was later extended by Tanaka and Edwards [45] to include the physical associations between the polymers. The network theory describes the real (G', storage modulus) and the imaginary (G'', loss modulus) parts of the complex viscoelastic shear modulus in terms of the Maxwell model, which is expressed by the following Eqs. (15) and (16):

$$G' = G_0 \frac{\omega^2\tau^2}{1+\omega^2\tau^2} \quad (15)$$

$$G'' = G_0 \frac{\omega\tau}{1+\omega^2\tau^2} \quad (16)$$

where, G_0 is the plateau modulus, τ is the relaxation time of the network and ω the angular frequency.

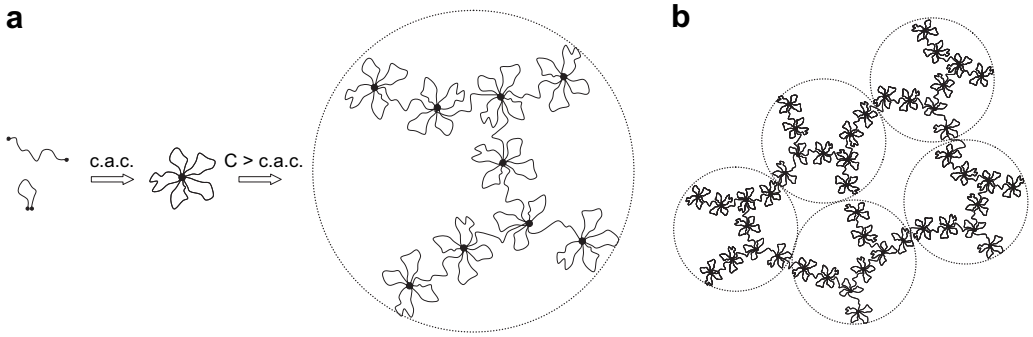

Fig. 11. Schematic representation of end-capped PEO self-assembling in dilute solutions forming flowers, clusters (a) and percolating clusters (b).

The plateau modulus is given by:

$$G_0 = \nu k_B T \quad (17)$$

where, ν is the number of elastically active chains in the network per unit volume, k_B is the Boltzmann constant and T is the absolute temperature.

Fig. 12 shows the typical frequency dependence of dynamic moduli (G' and G'') and complex viscosity (η^*) obtained with an aqueous solution of PEO20K-PDC at $C = 20\ g\ L^{-1}$ and $T = 20\ °C$. At low frequency, the complex moduli follow the Maxwellian behavior with respective slopes close to 1 and 2 for G'' and G', while the complex viscosity remains independent of frequency as expected for a Newtonian behavior. At higher frequencies, G' and G'' cross each other ($G_c = 28$ Pa) at a characteristic frequency ($\omega_c = 17$ rad/s) which is directly related to the relaxation time of the network: $\tau = 1/\omega_c = 0.06$ s. Above ω_c, the system becomes solid like and G' finally reaches a plateau value at $G_0 = 56$ Pa. It can be seen from Fig. 12 that the Maxwell model with a single relaxation time fits the experimental data very well in the whole range of frequencies and the same holds for all the polymer solutions at all concentrations ($C > C_g$) and temperatures investigated.

Above C_g, the plateau modulus rises rapidly due to the increasing fraction of elastically active chains ($x = G_0/nRT$ see Table 5). As we are dealing with adhesive flowerlike micelles, it is also interesting to define the fraction of elastically active micelles ($X = G_0 N_{agg}/nRT$) which gives an idea of the average connectivity between flowers. In this way, we can see that for $C \approx 2C_g$ most of flowerlike micelles are elastically active ($X \geq 1$) which means that they bridge, on average, at least two neighboring micelles. This transformation of loops into bridges is expected to end at higher concentrations ($C \geq 3C_g$) when flowers become closepacked and compressed [11,36].

Table 5
Viscoelastic characteristics of end-capped PEO in aqueous solution ($T = 20\ °C$)

Sample	PEO10K-PDC			PEO20K-PDC		
C (g L^{-1})	40	60	80	20	30	40
C/C_g	1.27	1.91	2.54	1.33	2.00	2.67
η (Pa s)	1.1	41	77	3.2	34	117
τ (s)	0.025	0.068	0.070	0.057	0.083	0.10
G_0 (Pa)	36	620	1130	56	408	1260
$x = G_0/nRT$	0.0036	0.042	0.058	0.023	0.11	0.26
$X = G_0 N_{agg}/nRT$	0.08	0.92	1.28	0.32	1.76	4.42

$N = C/M$ is the molar concentration of PEO chains (mol/m^3).

The main conclusions are summarized in Fig. 13, where the viscosity data have been rescaled using the reduced concentration C/C_g.

Taking into account the picture of adhesive flowers, it is tempting to probe the pertinence of the percolation theory to describe the sol–gel transition of PDC end-capped PEO.

3.3.3.2. Sol–gel transition. Initially developed for chemical gelation, the percolation theory also provides an interesting tool to describe the formation of physical gels, and it has been successfully applied to a wide variety of systems such as pectins/Ca^{2+}, poly(vinyl-chloride)/dioctyl phthalate, poly(vinyl alcohol)/borate and pluronic micelles [46–49]. An important fundamental feature of the percolation theory is the existence of a critical value p_c of p (bond formation probability in the bond percolation process or occupied probability of the site in the site percolation process) beyond which

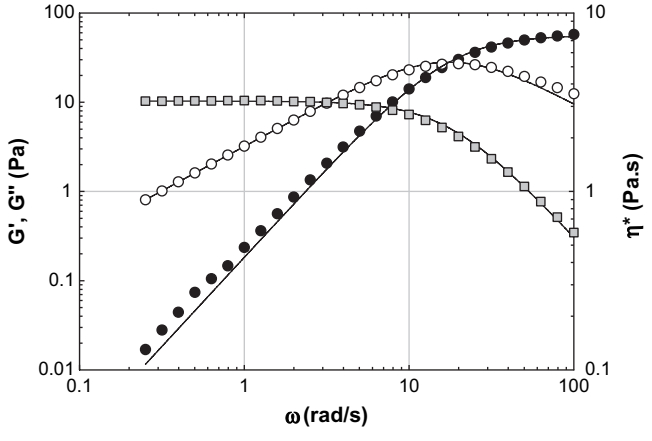

Fig. 12. Viscoelastic properties of PEO20K-PDC ($C = 20\ g\ L^{-1}$ and $T = 20\ °C$). G' (●), G'' (○) and η^* (■). The solid lines indicate the best fit of Maxwell model with a single element: $G_0 = 56$ Pa, $\tau = 0.057$ s and $\eta_0 = 3.2$ Pa s.

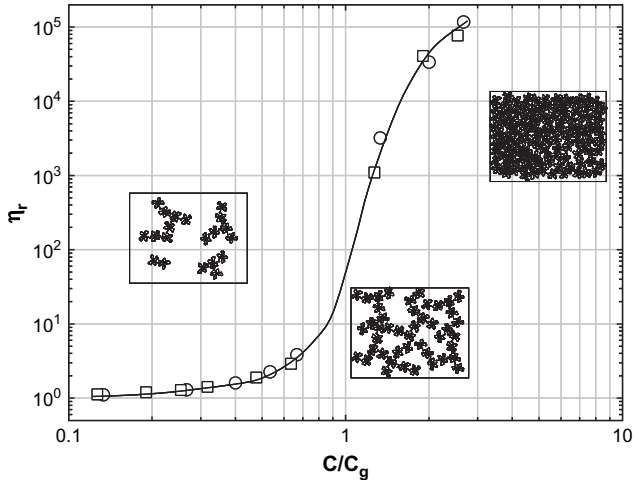

Fig. 13. Relative viscosity ($\eta_r = \eta_{solution}/\eta_{solvent}$) of PDC end-capped PEO in aqueous solution ($T = 20\ °C$) versus reduced concentration: PEO10K-PDC (○), PEO20K-PDC (□).

the probability of finding a percolating cluster (i.e., a cluster that spans the whole sample) is nonzero. Whereas below p_c the viscosity increases and diverges at the transition, above p_c, the viscosity is no longer useful in describing the system, and it is the increasing elastic modulus that is considered to follow the bond formation. Close to the gel point, the percolation theory predicts scaling relations for viscoelastic properties using ε, which is the distance from the gel point ($\varepsilon = |p - p_c|$). For a viscoelastic system characterized by a zero shear viscosity η_0 and a shear plateau modulus G_0, the exponents used to describe the singularities near the gel point are n, s and t given by [50]:

$$\text{Below the gel point } (p < p_c): \eta_0 \sim \varepsilon^{-s} \tag{18}$$

$$\text{At the gel point } (p = p_c): G' \sim G'' \sim \omega^{n} \tag{19}$$

$$\text{Above the gel point } (p > p_c): G_0 \sim \varepsilon^{t} \tag{20}$$

These parameters are related to each other by the following relation:

$$n = t/(s+t) \tag{21}$$

Various theoretical approaches try to describe the dynamics of branched structures near the gelation threshold. For instance we can mention the electrical analogy, with the formation of a percolating conductor network in an insulating medium, and the Rouse model which assumes no hydrodynamic interaction between polymers [50]. The main difference between these two models arises from the existence of dangling ends and loops in the percolating network that do not contribute to the elasticity. These defects are considered in the electrical analogy and omitted in the Rouse model.

In physical gelation, p depends on the cross-linking mechanism; it may be temperature, curing time, concentration, etc. In the present case, where gelation is expected to proceed through a site percolation process between adhesive flowers, the key parameter is the concentration of polymer. In the following, we will use the relative distance from the gel point

$$\varepsilon = |(C - C_g)/C_g| \tag{22}$$

which is more useful to draw a general comparison between different associating copolymers.

Even if C_m and C^* are very close, the scaling exponents reported in Table 6 clearly depend from the choice of the reference concentration (C_g), which should be normally defined by the conditions given in Eq. (19).

Nevertheless, a normalized picture of the percolation dynamics can be obtained by plotting the rheological data versus the relative distance to the gel point defined previously as: $C_g = (C_m + C^*)/2$ (see Fig. 14). This representation gives $t \cong 2$ which is close to the theoretical value given by the electrical analogy and to experimental exponents obtained for physical gels like calcium pectinate

Table 6
Experimental and theoretical scaling exponents related to Eqs. (18)–(21)

Experimental	$C_g = C_m$			$C_g = C^*$		
	s	t	n	s	t	n
PEO10K-PDC	1.2	1.7	0.6	0.9	2.3	0.7
PEO20K-PDC	0.9	2.3	0.7	1.4	1.5	0.5
Theoretical values	0.75	1.9	0.72	1.32	2.7	0.66
	Electric network analogy			Rouse model		

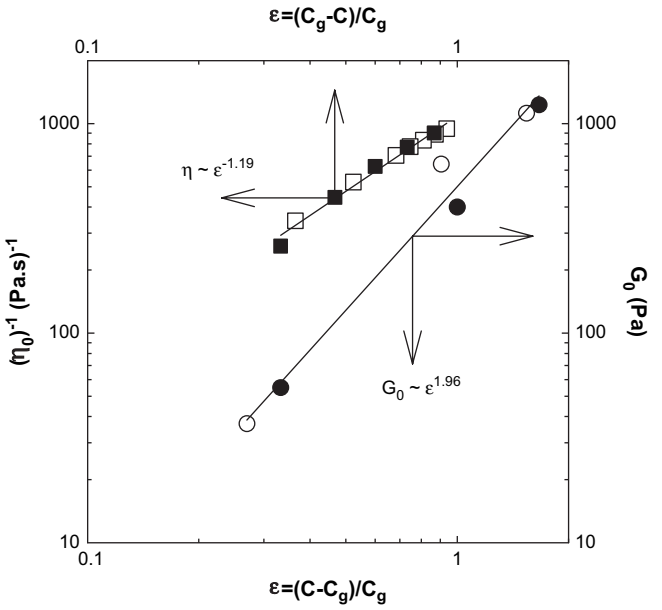

Fig. 14. Variations of Newtonian viscosity (η_0; squares) and plateau modulus (G_0; circles) with the relative distance from the gel point (ε) for PEO10K-PDC (hollow symbols) and PEO20K-PDC (filled symbols).

[46], hydrolyzed polyacrylamide complexed by Cr(III) [51] or casein gels [52].

The main purpose here is not to discuss on the validity of one model compared to another but to show that the percolation theory is pertinent to describe the gelation process of PDC end-capped PEO in aqueous solution. Following the initial picture given in Figs. 11 and 13, we can reasonably describe the gelation process of PDC end-capped PEO by the percolation of adhesive flowers which starts at $\varepsilon = 0$, at the gel point, and ends at about $\varepsilon \approx 1$, when the gel fraction is approximately unity [53]. Above C_g, a large increase of connectivity (G_0) is observed due to the strong shift from loops to bridges until $\varepsilon = 2$–3, where flowers start to fill all the space.

A very similar description has been done by Lafleche et al. [42] for mixtures of α- and α,ω-end-capped PEO, with a renormalization of η_0, G_0 and τ versus C/C_g. In the framework of the sol–gel transition of telechelic polymers it is generally assumed that before C_g, a high proportion of flowers are connected through primary bridges forming super bridges [11,42,54]. These super bridges contribute negatively to the relaxation time of the network as the escape of any primary chain end in the super bridge relaxes the stress and decreases τ. By crossing the percolation threshold, the proportion of super bridges is expected to drop rapidly and the opposite holds for the relaxation time. Theoretical predictions based on the mean field theory gives $\tau \sim \varepsilon^{\beta}$ with $\beta = 1$ [54,55]. In our case, we get a lower scaling exponent ($\beta \approx 0.3$) indicating that the number of primary chains is probably not so high in the vicinity of the sol–gel transition. This hypothesis seems quite reasonable if we take into account (1) the criterion suggested by Scanlan [56] and Case [57] that states that telechelic chains are elastically effective if their both ends are connected to junctions which have at least three paths to the infinite network and (2) the high functionality of PDC end-capped PEO flowers ($f = 35$–50) which increases their probability to share more than two bridges with neighboring micelles.

3.3.3.3. Time–temperature superposition. The characteristic time scale for the associations between polymers can be estimated from the value of the relaxation time (τ). Furthermore, this characteristic

time has been shown to increase exponentially with the size of the hydrophobic end groups [11], as described by the following relationship:

$$\tau = \tau_0 \exp(E_a/kT) \quad (23)$$

where, E_a is the activation energy or potential barrier, which depends both on the binding energy and on the additional activation barrier and τ_0 is a microscopic time corresponding to the sticker diffusion.

In order to get information concerning the activation energy E_a, the viscoelastic properties of polymer solutions have been studied at various temperatures ($T = 5, 10, 15, 20, 25$ and $30\,^{\circ}C$) and a Time–Temperature Superposition (TTS) has been applied to the whole set of data. An example is given in Fig. 15 with a solution of PEO20K-PDC ($C = 20\ g\ L^{-1}$) using a reference temperature $T_{ref} = 5\,^{\circ}C$. As we can see, the TTS procedure allows a very good superposition of the viscoelastic data by applying a frequency shift factor (a_T) and a modulus shift factor (b_T). These two parameters vary with the temperature and their temperature dependence has been fitted assuming a common Arrhenius behavior: $x_T \sim \exp(E_a/kT)$. These values, calculated for the two polymers studied at various concentrations, are reported in Table 7.

Except for PEO10K-PDC studied at a concentration very close to the sol–gel transition, all the systems give very similar activation energies for a_T ($E_a = (69 \pm 4)$ kJ mol^{-1}). This energy can be correlated to the potential barrier that a PDC sticker has to overcome to leave the hydrophobic aggregate. In the case of HEUR derivatives, which were studied in details by Annable and coworkers [11], a linear relation was obtained between the activation energy (E_a in kJ mol^{-1}) and the number of carbons (n_c) in the alkyl sticker:

$$E_a = 7n_c - 41 \quad (24)$$

By comparison with our data, activation energy $E_a \cong 70$ kJ mol^{-1} would correspond to linear alkyl chains with 16 carbons. This result is in very good agreement with the hydrophobicity expected for pentadecylcyclohexyl stickers. Concerning the vertical shift factor b_T, which describes the variation of the concentration of elastically active chains, a systematic decrease is observed with increasing temperature but also with decreasing concentration. This behavior can be attributed to the deswelling of flowerlike micelles upon heating (decrease of the hard sphere radius) as previously discussed in the neutron scattering session. Indeed, by decreasing the repulsions between PEO coronae, the temperature increases the density of fractal clusters and the percolation threshold (C_g), decreasing consequently the relative distance to the gel point (ε).

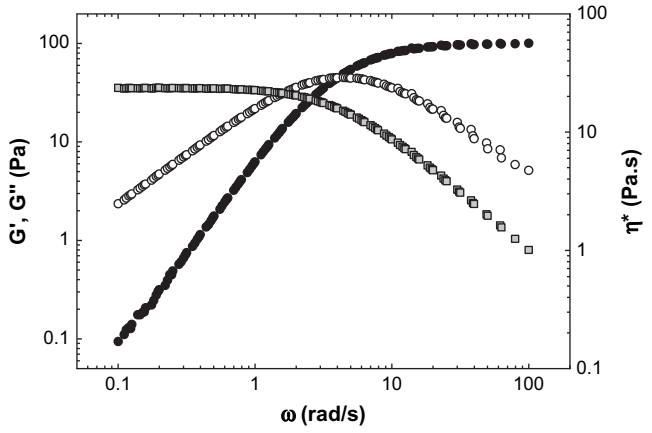

Fig. 15. Master curve obtained by TTS with a solution of PEO20K-PDC: G' (●), G'' (○) and η^* (■) ($C = 20\ g\ L^{-1}$, $T_{ref} = 5\,^{\circ}C$).

Table 7
Activation energies of horizontal (a_T) and vertical (b_T) shift factors obtained from the time–temperature superposition

Sample		PEO10K-PDC ($C_g = 32\ g\ L^{-1}$)			PEO20K-PDC ($C_g = 15\ g\ L^{-1}$)		
ε		0.27	0.91	1.54	0.33	1	1.67
a_T	E_a (kJ mol^{-1})	91	73	71	68	65	65
b_T	E_a (kJ mol^{-1})	51	24	14	26	17	15

The effect of temperature is more important since the concentration is close to C_g.

4. Conclusion

In the present work, we have shown that 1-isocyanato-3-pentadecylcyclohexane is a very good candidate for designing well controlled associating architectures. Starting with α,ω-hydroxy PEO of low polydispersity index, the addition of an excess of 1-PDC allows a good control of the end-capping reaction, irrespective of the size of the polymer chain. As expected from their primary structure, 1-PDC end groups self-associate in aqueous solution and give rise to connected architectures.

A reasonable picture of the self-assembly is obtained by fitting the scattering data with a simple model based on Gaussian stars interacting with an adhesive hard sphere potential. With four variables R_{Star}, N_{sti}, R_{HS}, and ζ^{-1}, this model quantitatively describes the main features of the micelles organization in the vicinity of the sol–gel transition. The aggregation number of end-capped PEO micelles falls from 25 to 17 with increasing molecular weight of PEO but it remains almost independent of the temperature between 20 and 40 °C. At the same time the temperature has a significant impact on the micelle coronas which become less repulsive upon heating.

The rheological measurements performed at low polymer concentrations clearly evidence the formation of loose structures (open clusters) built up from bridged micelles. The viscosity of dilute solutions of end-capped PEOs was successfully analyzed using the Fedors equation which allows the extrapolation of intrinsic viscosity, packing and overlap concentrations. The viscoelastic measurements performed at different concentrations and temperatures, show that the hierarchical self-assembly follows the rules of the percolation theory. The sol–gel transition takes place at the overlap concentration of clusters. In semi-dilute solutions, the viscoelastic data can be described by a Maxwell model with a single relaxation mode at all concentrations and temperatures. The activation energy for the disengagement rate of PDC from the micelle is about 70 kJ/mol, in good agreement with the size of the alkyl stickers. Finally, the lower critical solution temperature of PEO in water is responsible for the deswelling of micelle coronas upon heating and for the decreasing number of elastically active chains.

Acknowledgments

SRF fellowship to VSK by CSIR (India) and Sandwich thesis scholarship to VSK by French Embassy New Delhi is gratefully acknowledged. The financial support from DST, New Delhi is acknowledged. The authors also want to thank Dr. Annie Brûlet (LLB, CEA) for her helpful collaboration in SANS experiments.

References

[1] Glass JE, editor. Polymers in aqueous media: performance through association. Advances in chemistry series No. 223. Washington: American Chemical Society; 1989.
[2] Hoy KL, Hoy RC. U.S. Pat. 4 426 485; 1984.
[3] Alami E, Rawiso M, Isel F, Beinert G, Binane LW, François J, et al. Hydrophilic polymers: performance with environmental acceptability. In: Glass JE, editor.

Advances in Chemistry Series, vol. 248. Washington: American Chemical Society; 1996. p. 343.
[4] François J, Maitre S, Rawiso M, Sarazin D, Beinert G, Isel F. Colloids Surf A 1996;112:251.
[5] Jenkins RD. PhD Thesis, University of Lehigh; 1990.
[6] Tripathi A, Tam KC, McKinley GH. Macromolecules 2006;39:1981.
[7] François J, Beaudoin E, Borisov O. Langmuir 2003;19:10011.
[8] Lundberg D, Glass JE, Eley RR. J Rheol 1991;35:1255.
[9] Yekta A, Xu B, Duhamel J, Adiwidjaja H, Winnik MA. Macromolecules 1995;28:956.
[10] Xu B, Li L, Yekta A, Masoumi Z, Kanagalingam S, Winnik MA, et al. Langmuir 1997;13:2447.
[11] Annable T, Buscall R, Ettelai R, Whittlestone D. J Rheol 1993;37:695.
[12] Ng WK, Tam KC, Jenkins RD. J Rheol 2000;44:137.
[13] Kaczmarski JP, Glass JE. Macromolecules 1993;26:5149.
[14] Rangelov S, Tsvetanov C. Polym Bull 2001;46:471.
[15] Yao N, Jamieson AM. Polymer 2000;41:2925.
[16] Grassl B, Billon L, Borisov O, François J. Polym Int 2006;55:1169.
[17] Badiger MV, Kadam VS, Lele AK, Wadgaonkar PP, Hourdet D. Macromol Symp 2006;241:9.
[18] Shedge AS, Lele AK, Wadgaonkar PP, Hourdet D, Perrin P, Chassenieux C, et al. Macromol Chem Phys 2005;206:464.
[19] Cotton JP, Decker D, Farnoux B, Janninck G, Ober R, Picot C. Phys Rev Lett 1974;32:1170.
[20] Cabane B, Duplessix R. J Phys 1982;43:1529.
[21] Benoît H. J Polym Sci 1953;11:507.
[22] Daoud M, Cotton J, France P. J Phys 1982;43:531.
[23] Mortensen K, Brown W. Macromolecules 1993;26:4128.
[24] Liu Y, Chen SH, Huang JS. Macromolecules 1998;31:2236.
[25] Yang L, Alexandridis P. Langmuir 2000;16:4819.
[26] Serero Y, Aznar R, Porte G, Berret JF, Calvet D, Collet A, et al. Phys Rev Lett 1998;81:5584.
[27] Filali M, Aznar R, Svenson M, Porte G, Appell J. J Phys Chem 1999;103:7293.
[28] Beaudoin E, Borisov O, Lapp A, Billon L, Hiorns RC, François J. Macromolecules 2002;35:7436.
[29] Beaudoin E, Borisov O, Lapp A, François J. Macromol Symp 2002;189:89.
[30] Baxter RJ. J Chem Phys 1968;49:2770.
[31] Pham QT, Russel WB, Thibeault JC, Lau W. Macromolecules 1999;32:2996.
[32] Pham QT, Russel WB, Thibeault JC, Lau W. Macromolecules 1999;32:5139.
[33] Vorobyova O, Winnik MA, Lau W. Macromolecules 2001;17:1357.
[34] Vorobyova O, Yekta A, Winnik MA, Lau W. Macromolecules 1998;31:8998.
[35] Borbély S. Langmuir 2000;16:5540.
[36] Semenov AN, Joanny JF, Khokhlov AR. Macromolecules 1995;28:1066.
[37] Fedors RF. Polymer 1979;20:225.
[38] Dragan S, Ghimici L. Polymer 2001;42:2887.
[39] Juntao M, Bin L, Ping C, Hua D, Ronghua H. Polymer 2003;44:1281.
[40] Cathébras N, Collet A, Viguier M, Berret JF. Macromolecules 1998;31:1305.
[41] Gourier C, Beaudoin E, Duval M, Sarazin D, Maître S, François J. J Colloid Interface Sci 2000;230:41.
[42] Lafleche F, Durand D, Nicolaï T. Macromolecules 2003;36:1331.
[43] Bremer LGB, van Vliet T, Walstra P. J Chem Soc Faraday Trans 1989;85:3359.
[44] Green MS, Tobolsky A. J Chem Phys 1946;14:80.
[45] (a) Tanaka F, Edwards SF. J Non-Newtonian Fluid Mech 1992;43:247;
(b) Tanaka F, Edwards SF. J Non-Newtonian Fluid Mech 1992;43:273;
(c) Tanaka F, Edwards SF. J Non-Newtonian Fluid Mech 1992;43:289;
(d) Tanaka F, Edwards SF. Macromolecules 1992;25:1516.
[46] Axelos MAV, Kolb M. Phys Rev Lett 1990;64:1457.
[47] Te-Nijenhuis K. Adv Polym Sci 1996;130:1.
[48] Winters HH, Mours M. Adv Polym Sci 1997;134:165.
[49] Lobry L, Micali N, Mallamace F, Liao C, Chen S-H. Phys Rev E 1999;60:7076.
[50] Adam M, Lairez D. In: Addad JPC, editor. Physical properties of polymeric gels; 1996. p. 88.
[51] Allain C, Salomé L. Macromolecules 1990;23:981.
[52] Tokita M, Niki R, Hikichi K. J Chem Phys 1985;83:2583.
[53] Rubinstein M, Colby RH. Polymer physics. Oxford University Press; 2003. p. 197.
[54] Indei T. J Chem Phys 2007;127:144905.
[55] Rubinstein M, Semenov AN. Macromolecules 1998;31:1386.
[56] Scanlan J. J Polym Sci 1960;43:501.
[57] Case LC. J Polym Sci 1960;45:397.